Journal of Power Sources 237 (2013) 149–155

Contents lists available at SciVerse ScienceDirect

Journal of Power Sources

journal homepage: www.elsevier.com/locate/jpowsour

Improved electrochemical performance of $LiFePO_4$/C cathode via Ni and Mn co-doping for lithium-ion batteries

Hongbo Shu, Xianyou Wang*, Qiang Wu, Benan Hu, Xiukang Yang, Qiliang Wei, Qianqian Liang, Yansong Bai, Meng Zhou, Chun Wu, Manfang Chen, Aiwen Wang, Lanlan Jiang

Key Laboratory of Environmentally Friendly Chemistry and Applications of Ministry of Education, School of Chemistry, Xiangtan University, Hunan, Xiangtan 411105, China

HIGHLIGHTS

- Ni and Mn co-doping $LiFePO_4$/C are prepared firstly by a simple solid-state route.
- Ni and Mn co-doping can effectively improve the performance of $LiFePO_4$.
- $LiFe_{0.95}Ni_{0.02}Mn_{0.03}PO_4$/C shows the best rate capability and cycling stability.
- Ni and Mn co-doping is an effective way to improve the performance of material.

ARTICLE INFO

Article history:
Received 23 November 2012
Received in revised form
5 March 2013
Accepted 9 March 2013
Available online 19 March 2013

Keywords:
Lithium ion batteries
Lithium iron phosphate
Nickel and manganese co-doping
High-temperature solid-state route
Electrochemical performance

ABSTRACT

The pristine $LiFePO_4$/C and Ni and Mn co-doping $LiFe_{1-x-y}Ni_xMn_yPO_4$/C ($x = 0.01–0.04$; $y = 0.04–0.01$) composites are synthesized for the first time by a simple high-temperature solid-state route. The structure, morphology and electrochemical performance of the samples are characterized by X-ray diffraction (XRD), Fourier transform infrared (FTIR) spectra, scanning electron microscope (SEM), charge/discharge tests and electrochemical impedance spectroscopy (EIS). The results indicate that the Ni and Mn co-doping does not destroy the olivine structure of $LiFePO_4$, but it can stabilize the crystal structure, lengthen the Li–O bond, decrease charge transfer resistance, enhance Li ion diffusion velocity, and thus improve its cycling and high-rate capability of the $LiFePO_4$/C. Especially, the $LiFe_{0.95}Ni_{0.02}Mn_{0.03}PO_4$/C shows the best cycling stability and rate capability among all the doped samples. The first discharge capacity of $LiFe_{0.95}Ni_{0.02}Mn_{0.03}PO_4$/C is 145.4 mAh g^{-1} with the capacity retention ratio of 98.6% till 100 cycles at 1C. Even at a high rate of 10C, it still reveals a high discharge capacity of 115.2 mAh g^{-1}.

1. Introduction

Since the olivine $LiFePO_4$ was first reported by Goodenough and co-workers in 1997 [1], it has brought extensive interests over the past decade, due to its superior capacity retention, stable voltage platform, remarkable tolerance to overcharge and overdischarge, good thermal stability, excellent safety, nontoxicity and potentially low cost [2]. However, the poor electronic conductivity, ionic conductivity and ionic diffusivity of pure $LiFePO_4$ have hampered its extensive application in high-rate lithium ion batteries [3–5].

Up to the present, many effective approaches have been proposed to solve above problem. The approaches mainly involve $LiFePO_4$ coating with fine electronic conductive materials like carbon [6–9], reducing particle size [7,10], and $LiFePO_4$ doping with alien cations [11–13]. Among the above methods, alien cations doping at Li-site or Fe-site of $LiFePO_4$ is very convenient and effective to enhance the electrochemical properties of $LiFePO_4$ [12,14–16]. The first-principle calculation on $LiMPO_4$ (M = Fe, Mn, Co, and Ni) reveals that the lowest Li migration energy for the nonlinear pathway along the [010] channel is curved trajectory between Li sites, and with such one-dimensional pathway, long-range Li conduction may be easily blocked by Li site doping [17,18]. Therefore, Fe-site doping may be a more suitable strategy to enhance the intrinsic conductivity, and now great efforts have been devoted to investigate the doping effects at Fe-site on the physicochemical and electrochemical properties of $LiFePO_4$ [19,20]. In addition, an isovalent cation (such as Mg^{2+}, Cu^{2+}, Co^{2+} and so on) would easily occupy Fe sites of $LiFePO_4$, it could induce the crystal lattice distortion, provide more space for intercalation/deintercalation of Li^+, and thus improve the electrochemical properties

* Corresponding author. Tel.: +86 731 58292060; fax: +86 731 58292061.
E-mail address: wxianyou@yahoo.com (X. Wang).

0378-7753/$ – see front matter © 2013 Elsevier B.V. All rights reserved.
http://dx.doi.org/10.1016/j.jpowsour.2013.03.035

of $LiFePO_4$ [21–23]. Although many investigations have been done in order to enhance electrochemical performance of $LiFePO_4$, it has been rarely reported on isovalent cations co-doping at Fe sites of $LiFePO_4$.

In this work, $LiFePO_4$/C composites were prepared via a simple high-temperature solid-state method. In order to further effectively improve the electrochemical performance of $LiFePO_4$/C, the $LiFePO_4$/C sample with Ni and Mn co-doping was synthesized by high-temperature solid-state route. The effect of Ni and Mn co-doping with different amount on the structure, morphology and electrochemical property of $LiFePO_4$/C are studied in detail.

2. Experimental

2.1. Sample synthesis

Pristine $LiFePO_4$/C and $LiFe_{1-x-y}Ni_xMn_yPO_4$/C (x = 0.01, 0.02, 0.03 and 0.04; y = 0.04, 0.03, 0.02 and 0.01) powders were synthesized as follows: the stoichiometric amounts of Li_2CO_3 (AR), $FeC_2O_4{\cdot}2H_2O$ (AR), $NH_4H_2PO_4$ (AR), $Mn(CH_3COO)_2{\cdot}4H_2O$ (AR), $Ni(CH_3COO)_2{\cdot}4H_2O$ (AR) and sugar (AR) were mixed in ethanol and ball-mill for 6 h. Then the mixed slurry was dried at 80 °C in the oven. After drying, the mixture was calcined in Ar/H_2 (95:5 V%) atmosphere at 350 °C for 8 h. The yielded precursor powder was reground. The final product was obtained by heating the mixture at 700 °C for 15 h under Ar/H_2 (95:5 V%) atmosphere. Before increasing the temperature, the tube furnace was evacuated for 30 min in advance. The heating rate was 5 °C min^{-1}.

2.2. Materials characterization

The phase identification of the samples was performed with a diffractometer (D/Max-275, Japan) using Cu Kα radiation (λ = 1.54178 Å) and a graphite monochromator at 40 kV, 250 mA. The diffraction data for Rietveld refinement were obtained at 2θ = 10–70°, with a step size of 0.02° [24]. The FTIR spectra of $LiFePO_4$/C were recorded on a Perkin–Elmer Spectrum One FTIR Spectrometer. The weight percentage of carbon in the samples was determined by a C, H, N Analyser model 1106 Carlo Erba Strumentazione. The surface morphology of the samples was observed using the JSM-5600LV SEM (JEOL, Japan) equipped with an energy dispersive spectrometer (EDS).

2.3. Electrochemical measurements

The electrochemical tests of the as-synthesized samples were carried out using button cells assembled in an argon-filled glove box. In all cells, the cathode was consisted of a mixture of active material (80 wt.%), acetylene black (5 wt.%), graphite (5 wt.%) and polyvinylidene fluoride (PVDF) as binder agent (10 wt.%); lithium was served as counter and reference electrodes; a Celgard 2400 was used as separator, and the electrolyte was 1 M $LiPF_6$ solution in ethylene carbonate (EC)–dimethyl carbonate (DMC) (1:1, V/V). Charge-discharge measurement was carried out in Neware battery test system BTS-XWJ-6.44S-00052 (Neware, Shenzhen, China) at different current densities between 2.3 and 4.2 V vs. Li/Li^+. Electrochemical impedance spectroscopy (EIS) measurements were performed with

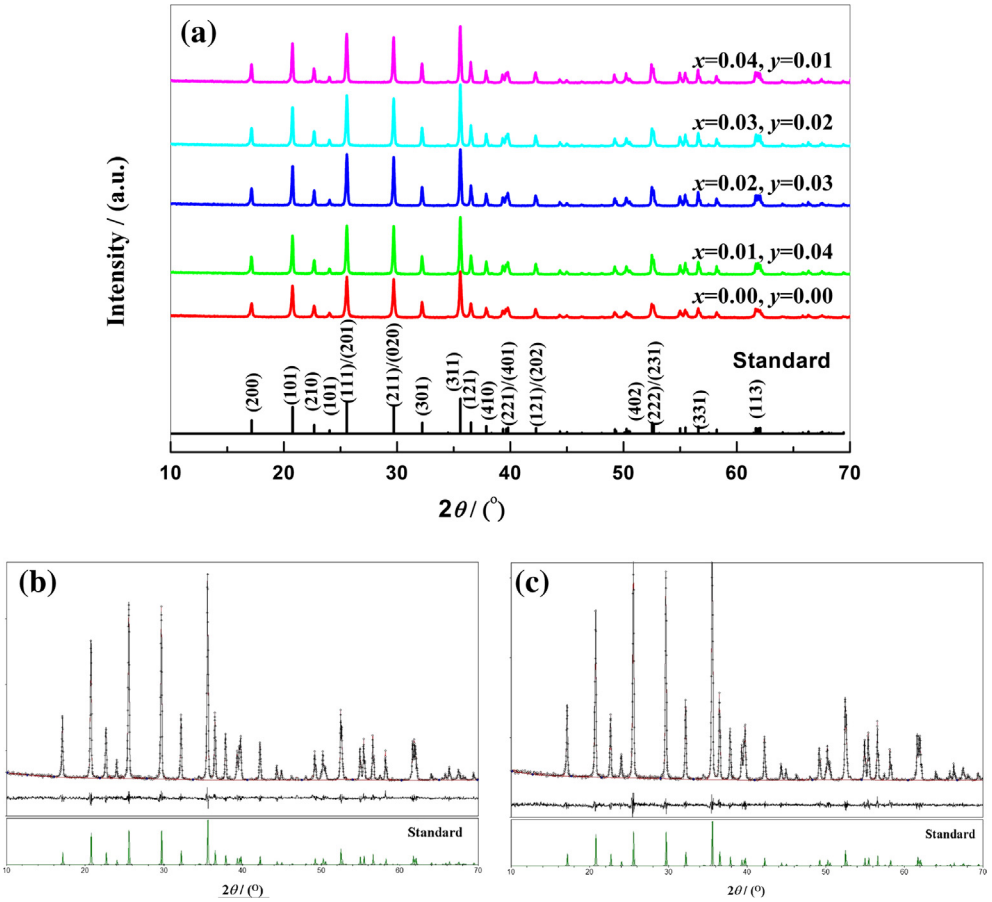

Fig. 1. (a) XRD patterns of $LiFe_{1-x-y}Ni_xMn_yPO_4$/C (x = 0.01, 0.02, 0.03 and 0.04; y = 0.04, 0.03, 0.02 and 0.01); Rietveld refinements of X-ray diffraction patterns for (b) $LiFePO_4$/C and (c) $LiFe_{0.95}Ni_{0.02}Mn_{0.03}PO_4$/C.

Table 1
Cell parameters of $LiFePO_4$/C and $LiFe_{1-x-y}Ni_xMn_yPO_4$/C (x = 0.01, 0.02, 0.03 and 0.04; y = 0.04, 0.03, 0.02 and 0.01).

Samples	a (Å)	b (Å)	c (Å)	V (Å^3)
$x = 0.00$, $y = 0.00$	10.3395	6.0150	4.6979	292.1722
$x = 0.01$, $y = 0.04$	10.3360	6.0117	4.6951	291.7391
$x = 0.02$, $y = 0.03$	10.3373	6.0118	4.6949	291.7682
$x = 0.03$, $y = 0.02$	10.3390	6.0134	4.6947	291.8814
$x = 0.04$, $y = 0.01$	10.3382	6.0135	4.6951	291.8886

a VersaSTAT3 electrochemical workstation (Princeton, America), the excitation voltage applied to the cells was 5 mV and the frequency ranged from 0.01 Hz to 100 kHz. All the electrochemical measurements were carried out at room temperature.

3. Results and discussion

The XRD patterns of the samples are shown in Fig. 1. All dominant diffraction lines of samples can be indexed as an olivine phase with an ordered orthorhombic structure belonging to the space group *Pnma*, indicating a perfect crystallinity of the as-synthesized samples. Besides, there is no evidence for the formation of amorphous carbons. The content of the residual carbon is about 4.8 wt.%, determined by element analysis. Furthermore, the Ni and Mn co-doping also does not change the crystal structure of the samples. The co-doping of Ni and Mn would be preferred to occupy Fe sites because the phase of $LiNiPO_4$ and $LiMnPO_4$ is structurally same to olivine $LiFePO_4$ [1,25–27]. The lattice parameters of the as-synthesized samples are calculated based on the XRD analysis listed in Table 1. As being shown, the value of lattice parameters decreases slightly with Ni and Mn co-doping. It is in agreement with the fact that radius of Ni ion (r = 0.69 Å) and Mn ion (r = 0.60 Å) is smaller than that of Fe ion (r = 0.74 Å) in octahedral coordination.

The XRD patterns of $LiFePO_4$/C and $LiFe_{0.95}Ni_{0.02}Mn_{0.03}PO_4$/C were further analyzed by Rietveld refinements shown in Fig. 1(b) and (c). The results of refinement for both samples are listed in Table 2. In this work, the refinement was carried out by assumption of Ni and Mn at Fe site. The reliability factor R_{wp} of the refinement showed in Table 2 is around 8%, demonstrating that the results are reliable. The variational lattice constant and credible reliability factor R_{wp} of the refinement showed in Tables 1 and 2 indicate that the Ni and Mn ions have been successfully doped into the $LiFePO_4$ phase [28,29]. In addition, the average lengths of the Fe–O and P–O bond for $LiFe_{0.95}Ni_{0.02}Mn_{0.03}PO_4$/C are shorter, suggesting that $LiFe_{0.95}Ni_{0.02}Mn_{0.03}PO_4$/C has a more stable structure for the charge/discharge reaction, and consequently has better cyclic performance [21,30]. Moreover, the average lengths of Li–O bond of $LiFe_{0.95}Ni_{0.02}Mn_{0.03}PO_4$/C illustrated in Table 2 are lengthened. A longer Li–O bond has a smaller binding energy, leading to easy migration of Li ion due to the reduction of the energy barrier, which will be beneficial to the electrochemical performance of cathode materials, especially under the high-C rate [27–29].

Table 2
Structural parameters obtained from XRD Rietveld refinement for $LiFePO_4$/C and $LiFe_{0.95}Ni_{0.02}Mn_{0.03}PO_4$/C.

Samples	$LiFePO_4$/C	$LiFe_{0.95}Ni_{0.02}Mn_{0.03}PO_4$/C
Lattice bond/Å		
Fe–O(1) × 1	2.2086	2.2070
Fe–O(2) × 1	2.1032	2.0890
Fe–O(3) × 2	2.0612	2.0588
Fe–O(3) × 2	2.2592	2.2499
Fe–O average	2.1581	2.1512
P–O(1) × 1	1.4406	1.4019
P–O(2) × 1	1.4941	1.4897
P–O(3) × 2	1.4555	1.4836
P–O average	1.4634	1.4584
Li–O(1) × 2	2.1543	2.1585
Li–O(2) × 2	2.0890	2.0907
Li–O(3) × 2	2.1805	2.1889
Li–O average	2.1413	2.1460
Reliability factors/%		
R_{wp}	7.97	7.76

The local environment of cations in a lattice of close-packed oxygen atoms can be estimated by FTIR spectrum because of the sensitivity of vibration modes of cations [31]. The effect of Ni and Mn on the crystal structure of $LiFePO_4$ is investigated by the FTIR spectra in Fig. 2. The characteristic peaks of MnO (production of $Mn(CH_3COO)_2{\cdot}4H_2O$) around 833 and 796 cm^{-1} [32] and NiO (production of $Ni(CH_3COO)_2{\cdot}4H_2O$) approximately 450 and 562 cm^{-1} [33] are not found in Fig. 2. It suggests that the MnO and NiO do not produce. Combined with XRD and FTIR, it can be indicated that the Ni and Mn successfully incorporated into the lattice of $LiFePO_4$. Besides, the effect of Ni and Mn co-doping on lattice of $LiFePO_4$ can be analyzed. The peaks of FTIR spectra for $LiFePO_4$/C composite locate at 463, 547, 638, 966, and 1043 cm^{-1}, which attributed to bending vibration and stretching vibration of tetrahedral $(PO_4)^{3-}$ ion [21,34]. All of the Ni and Mn co-doping $LiFe_{1-x-y}Ni_xMn_yPO_4$/C (x = 0.01–0.04; y = 0.04–0.01) samples are similar to $LiFePO_4$/C which contains five FTIR spectra peaks of $(PO_4)^{3-}$ ion shown in Fig. 2. However, the peaks of $LiFePO_4$/C with Ni and Mn co-doping shift to slightly higher band numbers than those of $LiFePO_4$/C. It indicates that the stability of the structure of the $LiFePO_4$ has been enhanced by Ni and Mn co-doping, which will be beneficial to cyclic performances of the $LiFePO_4$ [21,35].

Fig. 3 shows the morphologies of the as-prepared samples. As shown in Fig. 3a, the $LiFePO_4$/C is composed of irregular particles, which aggregate severely with a broad particle size distribution of 0.1–2.2 μm. However, the particle size, particle size distribution and particles agglomeration are relatively reduced after Ni and Mn co-doping. It suggests that the Ni and Mn co-doping can affect particles morphology. The reduction of particle size can shorten the diffusion path of the lithium ion as well as increase the electrochemical activation area, which is beneficial to improve the electrochemical performance of the material. The EDS result of $LiFe_{0.95}Ni_{0.03}Mn_{0.02}PO_4$/C in Fig. 4 indicates that the element composition of particle includes Fe, P, O, C, Ni and Mn, thus no other impurity is introduced to the as-prepared samples during the preparation process.

The charge/discharge curves of the samples between 2.3 and 4.2 V at a rate of 0.1 C (17 mA g^{-1}) are shown in Fig. 5. All of the

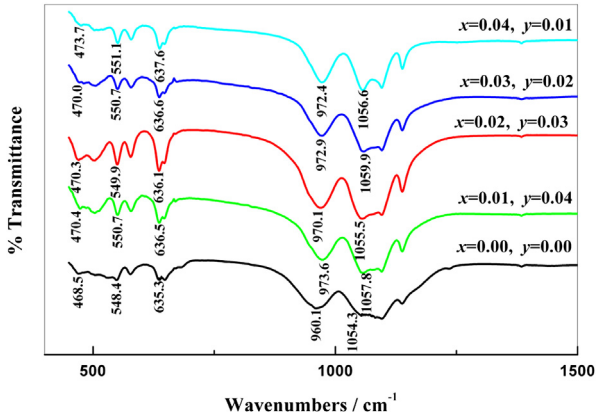

Fig. 2. FTIR spectra of $LiFePO_4$/C and $LiFe_{1-x-y}Ni_xMn_yPO_4$/C (x = 0.01, 0.02, 0.03 and 0.04; y = 0.04, 0.03, 0.02 and 0.01).

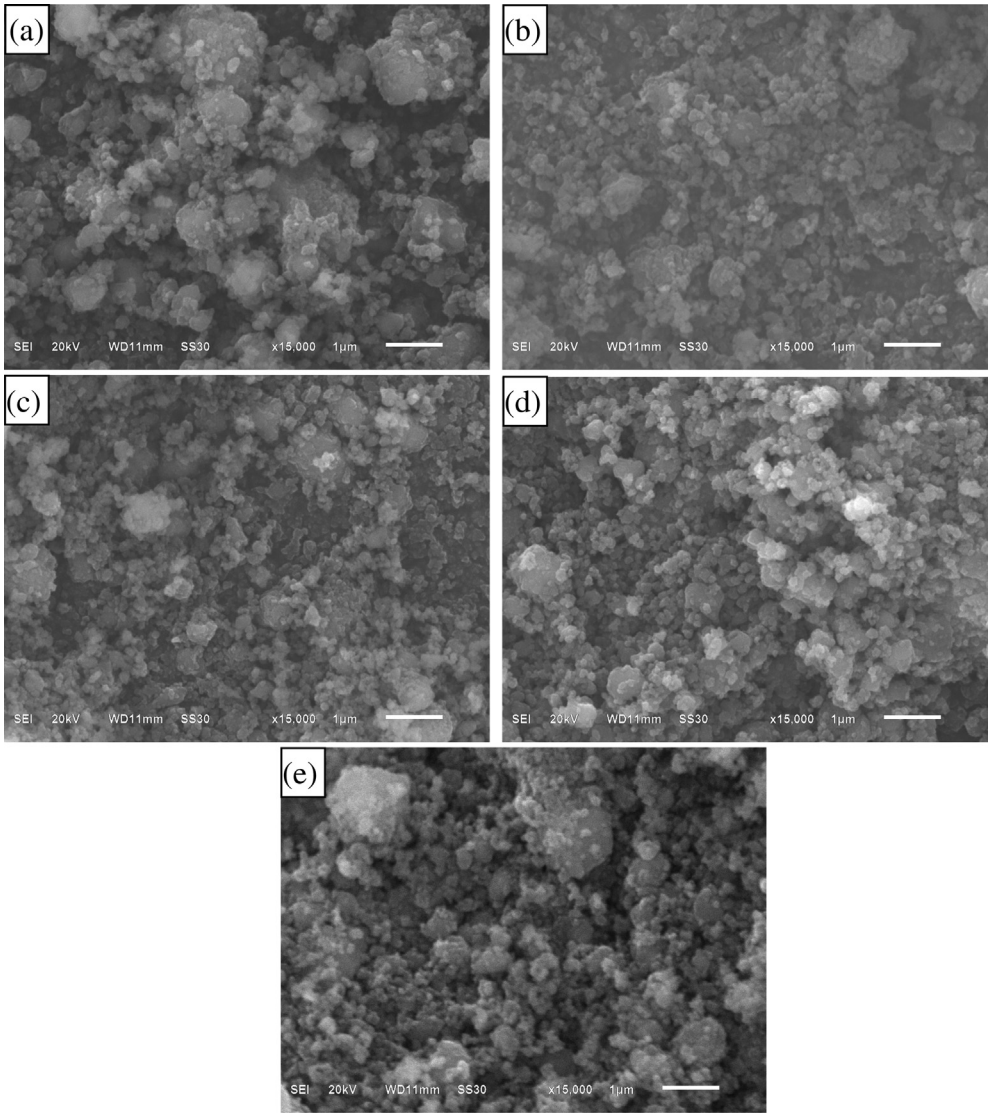

Fig. 3. SEM images of $LiFe_{1-x-y}Ni_xMn_yPO_4/C$. (a) $x = 0.00$, $y = 0.00$; (b) $x = 0.01$, $y = 0.04$; (c) $x = 0.02$, $y = 0.03$; (d) $x = 0.03$, $y = 0.02$; (e) $x = 0.04$, $y = 0.01$.

charge/discharge curves consist of a charge and discharge voltage plateaus at around 3.5 V and 3.4 V, which are the main characteristic of the two-phase reaction based on the redox couple of Fe^{2+}/Fe^{3+} during lithium-ion extraction and insertion process [29]. The potential interval between charge and discharge voltage plateaus for the samples is showed in insert of Fig. 5. It is found that the potential interval is effectively improved by Ni and Mn co-doping, indicating that the $LiFePO_4/C$ with Ni and Mn co-doping has the higher reaction kinetics than $LiFePO_4/C$ [36]. Especially,

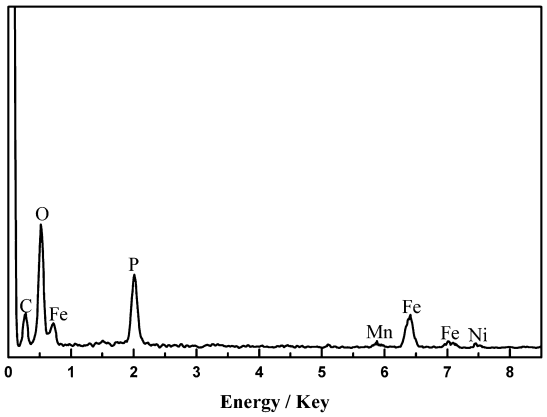

Fig. 4. EDS map of $LiFe_{0.95}Ni_{0.02}Mn_{0.03}PO_4/C$.

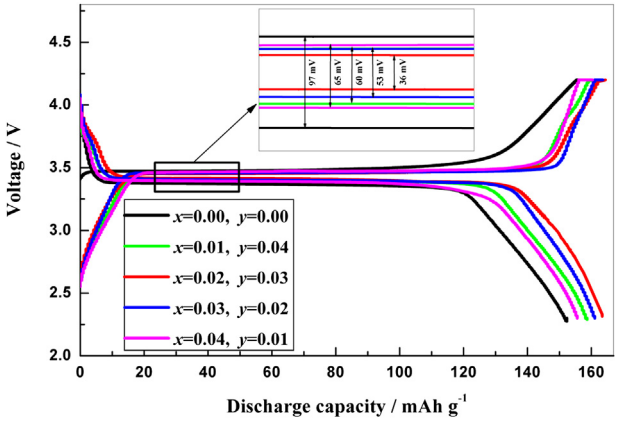

Fig. 5. Charge/discharge curves of $LiFePO_4/C$ and $LiFe_{1-x-y}Ni_xMn_yPO_4/C$ ($x = 0.01$, 0.02, 0.03 and 0.04; $y = 0.04$, 0.03, 0.02 and 0.01) at 0.1 C.

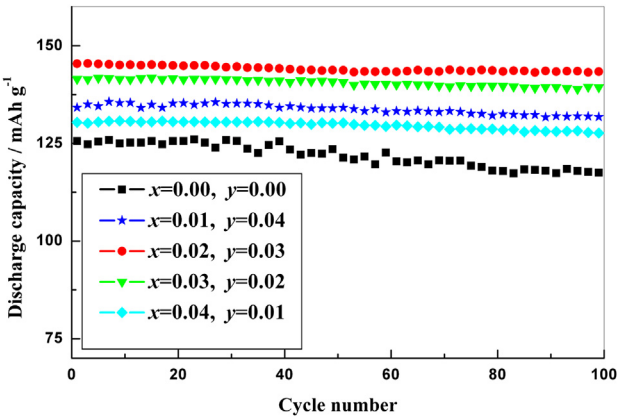

Fig. 6. The cycle performance of $LiFePO_4$/C and $LiFe_{1-x-y}Ni_xMn_yPO_4$/C (x = 0.01, 0.02, 0.03 and 0.04; y = 0.04, 0.03, 0.02 and 0.01) at 1 C.

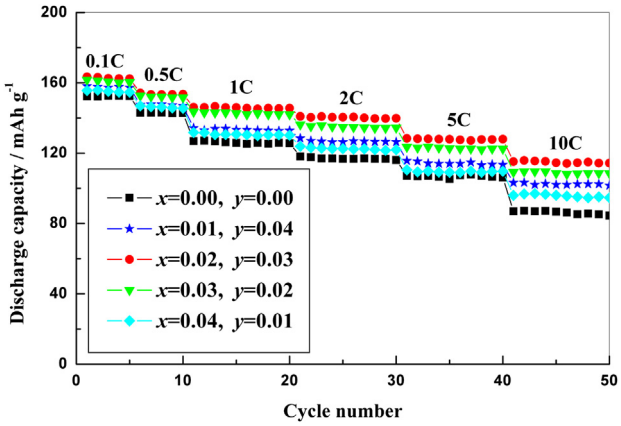

Fig. 7. The cycle performance of $LiFePO_4$/C and $LiFe_{1-x-y}Ni_xMn_yPO_4$/C (x = 0.01, 0.02, 0.03 and 0.04; y = 0.04, 0.03, 0.02 and 0.01) at different current rates.

$LiFe_{0.95}Ni_{0.02}Mn_{0.03}PO_4$/C shows the lowest polarization potential (36 mV) and the highest discharge capacity (164.0 mAh g^{-1}) at a rate of 0.1 C among all the samples.

The cycling life curves of the samples at 1 C are exhibited in Fig. 6. The cycle performance of the samples obtained from Fig. 6 is listed in Table 3. It is found that the discharge specific capacity and cycling performance of $LiFePO_4$/C is markedly improved by the Ni and Mn co-doping. Particularly, the $LiFe_{0.95}Ni_{0.02}Mn_{0.03}PO_4$/C exhibits the highest capacity and the best cycling performance among all the samples, it delivers an initial capacity of 145.4 mAh g^{-1} and possesses the capacity retention (Table 2) of 98.6.3% after 100 cycles at 1C.

Different discharge rates from 0.1 to 10C rates stepwise are applied to investigate the high-rate capability of the samples. The cycling performances of the samples at different current densities are shown in Fig. 7. Table 3 displays the rate capacity retention ratios of the samples compared to 0.1C. It is found from Fig. 7 and Table 3 that Ni and Mn co-doping enhances the rate capability of $LiFePO_4$/C. The $LiFe_{0.95}Ni_{0.02}Mn_{0.03}PO_4$/C reveals the best rate capability among all the samples. The decreases of discharge capacity of $LiFe_{0.95}Ni_{0.02}Mn_{0.03}PO_4$/C are less than those of other samples when the discharging current is increased from 0.1C to 10C. The $LiFe_{0.95}Ni_{0.02}Mn_{0.03}PO_4$/C delivers a discharge capacity of 154.2 (0.5C), 146.1 (1C), 140.9 (2C) and 128.4 (5C) mAh g^{-1}, the capacity retention rate is about 94.4%, 89.4%, 86.2% and 78.6%, compared to 0.1C, respectively. Even at 10C (1700 mA g^{-1}), the discharge capacity of $LiFe_{0.95}Ni_{0.02}Mn_{0.03}PO_4$/C is still as high as 115.2 mAh g^{-1} and the capacity retention rate is as high as about 70.5% of that of 0.1C. Apparently, these data with the same fabrication of electrodes composition are obviously higher than the results reported by other groups [37–39].

EIS is used to further analyze the effect of the Ni and Mn co-doping on the electrode reaction impedance. Before EIS tests, the cells are cycled for a several cycles. The potential obtained the Nyquist plots is about 3.0 V. The impedance spectra of samples are shown in Fig. 8a. Usually, an intercept in the high frequency region of the Z' real axis corresponds to the ohmic resistance (R_s), which represents the resistance of the electrolyte and electrode material. The semicircle in the middle frequency range indicates the charge transfer resistance (R_{ct}). The inclined line in the low frequency represents the Warburg impedance (Z_w), which is associated with lithium-ion diffusion in the $LiFePO_4$ particles.

The lithium-ion diffusion coefficient can be calculated according to the following equation [40–43]:

$$D = \frac{R^2T^2}{2A^2n^4F^4c^2\sigma_w^2} \quad (1)$$

where R is the gas constant, T is the absolute temperature, A is the surface area of the cathode, n is the number of electrons per molecule during oxidization, F is the Faraday constant, C is the concentration of lithium-ion, and σ_w is the Warburg factor which is relative with Z'.

$$Z\prime = R_s + R_{ct} + \sigma_w\omega^{-1/2} \quad (2)$$

where R_s is the resistance of the electrolyte and electrode material, R_{ct} is the charge transfer resistance and ω is the angular frequency in the low frequency region.

A simplified equivalent circuit model, which is constructed to analyze the impedance spectra is revealed in Fig. 8b. A constant phase element CPE in Fig. 8b represents the double layer capacitance and passivation film capacitance [39]. The parameters of the equivalent circuit are recorded in Table 4. The relationship plot between Z_{re} and reciprocal square root of the angular frequency ($\omega^{-1/2}$) at low-frequency region is shown in Fig. 8c. The lithium-ion

Table 3
The comparison of electrochemical property of the $LiFePO_4$/C and $LiFe_{1-x-y}Ni_xMn_yPO_4$/C (x = 0.01, 0.02, 0.03 and 0.04; y = 0.04, 0.03, 0.02 and 0.01).

Samples	1C (mAh g^{-1})			R_1[a] (%)						
	1th	100th	R_2[b] (%)	0.1C (mAh g^{-1})	0.1C	0.5C	1C	2C	5C	10C
x = 0.00, y = 0.00	125.6	117.0	93.2	152.3	100	93.9	83.3	77.6	70.5	57.1
x = 0.01, y = 0.04	134.2	130.8	97.5	158.1	100	93.3	85.0	81.3	73.2	62.3
x = 0.02, y = 0.03	145.4	143.4	98.6	163.4	100	94.4	89.4	86.2	78.6	70.5
x = 0.03, y = 0.02	141.5	138.9	98.2	161.1	100	94.7	89.1	84.6	76.7	67.8
x = 0.04, y = 0.01	130.4	126.5	97.0	155.6	100	94.4	83.8	79.6	71.0	61.7

[a] Capacity retention ratios of samples compared to the first cycle at 1C.
[b] Capacity retention ratios of samples compared to the 0.1C at different C rate.

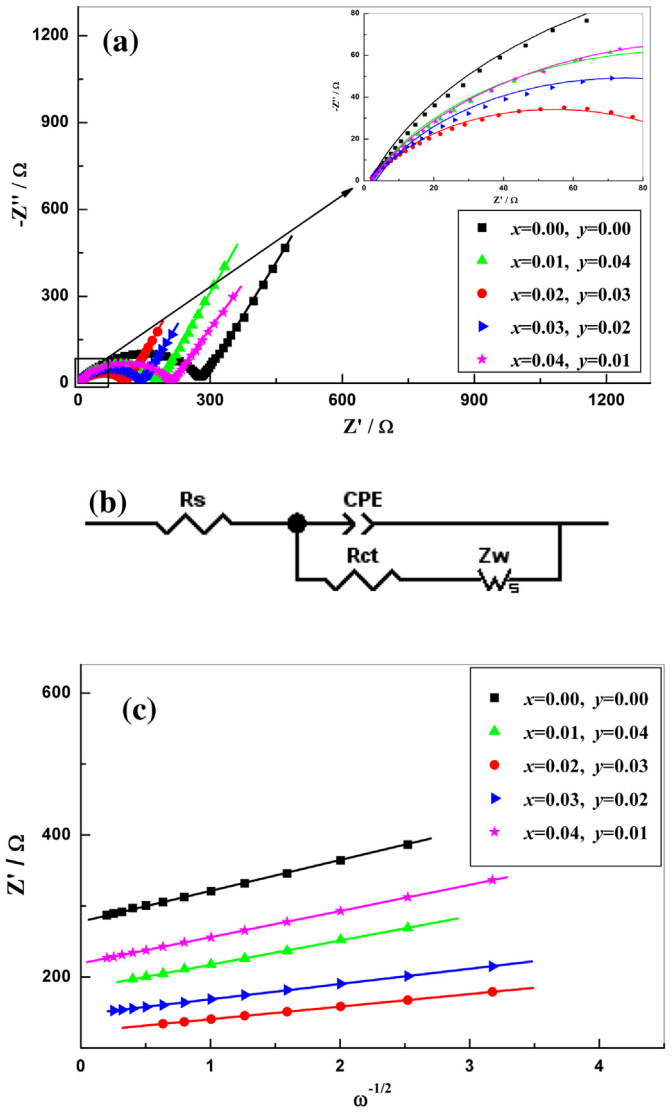

Fig. 8. (a) The impedance spectra of $LiFePO_4$/C and $LiFe_{1-x-y}Ni_xMn_yPO_4$/C (x = 0.01, 0.02, 0.03 and 0.04; y = 0.04, 0.03, 0.02 and 0.01). (b) Equivalent circuit used for fitting the experimental EIS data. (c) The relationship plot between Z_{re} and $\omega^{-1/2}$ at low-frequency region.

diffusion coefficients (D_{Li}) of the samples calculated by Eqs. (1) and (2) are listed in Table 4. The D_{Li} of $LiFe_{1-x-y}Ni_xMn_yPO_4$/C (x = 0.00, y = 0.00; x = 0.01, y = 0.04; x = 0.02, y = 0.03; x = 0.03, y = 0.02 and x = 0.04, y = 0.01) are 5.06×10^{-14}, 8.33×10^{-14}, 3.01×10^{-13}, 2.11×10^{-13} and 7.15×10^{-14}, respectively, which are higher than the previous reports (approximately 10^{-15} cm^2 s^{-1}) [41–43]. Apparently, the R_{ct} for the $LiFe_{0.95}Ni_{0.02}Mn_{0.03}PO_4$/C is the least and lithium-ion diffusion coefficient is the highest among all the samples.

Table 4
Electrode kinetic parameters obtained from equivalent circuit fitting of experimental data for $LiFePO_4$/C and $LiFe_{1-x-y}Ni_xMn_yPO_4$/C (x = 0.01, 0.02, 0.03 and 0.04; y = 0.04, 0.03, 0.02 and 0.01).

Samples	R_s (Ω)	R_{ct} (Ω)	D_{Li} (cm^2 s^{-1})	σ (S cm^{-1})
x = 0.00, y = 0.00	2.5	280.3	5.06×10^{-14}	6.36×10^{-5}
x = 0.01, y = 0.04	2.6	180.8	8.33×10^{-14}	9.86×10^{-5}
x = 0.02, y = 0.03	2.2	104.2	3.01×10^{-13}	1.71×10^{-4}
x = 0.03, y = 0.02	2.4	143.1	2.11×10^{-13}	1.25×10^{-4}
x = 0.04, y = 0.01	2.7	210.5	7.15×10^{-14}	8.47×10^{-5}

Besides, the electronic conductivity σ is calculated from the equation [36,41,42]:

$$\sigma = \frac{1/R_{ct}}{A/t} \quad (3)$$

Herein, t is the thickness of the electrode. It can be seen from Table 4 that the $LiFe_{0.95}Ni_{0.02}Mn_{0.03}PO_4$/C has the highest electronic conductivity σ among all the samples. Since the $LiFe_{0.95}Ni_{0.02}Mn_{0.03}PO_4$/C has the least particle size, the diffusion length of Li^+ is much shorter, which facilitates fast Li^+ insertion/extraction and improves lithium ion diffusion rate. Besides, Ni and Mn co-doping (x = 0.02, y = 0.03) have an inductive effect in the lattice, which can increase the disorder degree of the lattice and create the defects in $LiFePO_4$/C [21,23]. Accordingly, the carrier concentration is greatly enhanced, and the electronic conductivity of $LiFe_{0.95}Ni_{0.02}Mn_{0.03}PO_4$/C is effectively improved.

4. Conclusions

The well crystallized $LiFe_{1-x-y}Ni_xMn_yPO_4$/C (x = 0.01–0.04; y = 0.04–0.01) composites are successfully prepared via a simple high-temperature solid-state route. The Ni and Mn ions have successfully been doped into the $LiFePO_4$ phase. It can enhance the structural stability of $LiFePO_4$, lengthen the Li–O bond, modify the particle morphology, decrease charge transfer resistance, enhance electronic conductivity and Li ion diffusion velocity of $LiFePO_4$ and therefore clearly improve its cycling and high-rate capability. Peculiarly, the $LiFe_{0.95}Ni_{0.02}Mn_{0.03}PO_4$/C shows the best cycling stability and rate capability properties among all the samples. Therefore, the Ni and Mn co-doping is an effective approach to achieve excellent electrochemical performance for the phosphate positive materials.

Acknowledgments

This work was financially supported by the National Natural Science Foundation of China under project No. 20871101, Joint Fund of Natural Science of Hunan Province and Xiangtan City under project No. 09BG005, Industrial Project of Colleges and Universities of Hunan Province under project No. 10CY005. Project of Condition Research of Hunan Province under project No. 2010TC2004 and Colleges and Universities in Hunan Province plans to graduate research and innovation under project No. CX2011B268.

References

[1] A.K. Padhi, K.S. Nanjundaswamy, J.B. Goodenough, J. Electrochem. Soc. 144 (1997) 1188.
[2] L.X. Yuan, Z.H. Wang, W.X. Zhang, J.B. Goodenough, Energy Environ. Sci. 4 (2011) 269.
[3] H.C. Shin, K.Y. Chung, W.S. Min, D.J. Byun, H. Jang, B.W. Cho, Electrochem. Commun. 10 (2008) 536.
[4] C.W. Wang, A.M. Sastry, K.A. Striebel, J. Electrochem. Soc. 152 (2005) A1001.
[5] P.P. Prosini, M. Lisi, D. Zane, M. Pasquali, Solid State Ionics 148 (2002) 45.
[6] J.M. Chen, C.H. Hsu, Y.R. Lin, M.H. Hsiao, G.T.K. Fey, J. Power Sources 184 (2008) 498.
[7] D. Choi, P.N. Kumta, J. Power Sources 163 (2007) 1064.
[8] Y. Shi, S.L. Chou, J.Z. Wang, D. Wexler, Y.P. Wu, J. Mater. Chem. 22 (2012) 16465.
[9] J.W. Zhang, L.H. Zhuo, L.L. Zhang, C.Y. Wu, X.B. Zhang, J. Mater. Chem. 21 (2012) 6975.
[10] K. Saravanan, M.V. Reddy, P. Balaya, H. Gong, B.V.R. Chowdari, J. Mater. Chem. 19 (2009) 605.
[11] L. Bilecka, A. Hintennach, M.D. Rossell, D. Xie, J. Mater. Chem. 21 (2011) 5881.
[12] Z.L. Wang, S.R. Sun, D.G. Xia, J. Phys. Chem. C 112 (2008) 17450.
[13] Y.C. Ge, X.D. Yan, J. Liu, Electrochim. Acta 55 (2010) 5886.
[14] X. Zhao, X.Z. Tang, L. Zhang, M.S. Zhao, Electrochim. Acta 55 (2010) 5899.
[15] C.L. Hu, H.H. Yi, H.S. Fang, Int. J. Electrochem. Sci. 5 (2010) 1457.
[16] H. Liu, C. Li, Q. Cao, J. Solid State Electrochem. 12 (2008) 1017.
[17] M.S. Islam, D.J. Driscoll, Chem. Mater. 17 (2005) 5085.

[18] C.Y. Ouyang, S.Q. Shi, Z.X. Wang, J. Phys. Condens. Matter 16 (2004) 2265.
[19] Y.X. Wen, L.M. Zeng, Z.F. Tong, J. Alloys Compd. 416 (2006) 206.
[20] J. Ma, B.H. Li, H.D. Du, Electrochim. Acta 56 (2011) 7385.
[21] Y. Lu, J.C. Shi, Z.P. Guo, Q.S. Tong, W.J. Huang, J. Power Sources 194 (2009) 786.
[22] J. Ma, B.H. Li, H.D. Du, C.J. Xu, F.Y. Kang, J. Solid State Electrochem. 16 (2012) 1.
[23] D. Arumugam, K.G. Paruthimal, P. Manisankar, J. Solid State Electrochem. 13 (2009) 301.
[24] Z.J. Wu, H.F. Yue, L.S. Li, B.F. Jiang, X.R. Wu, P. Wang, J. Power Sources 195 (2010) 2888.
[25] A. Yamada, Y. Kudo, K.Y. Liu, J. Electrochem. Soc. 148 (2001) A1153.
[26] K.W. Nam, X.J. Liu, W.S. Yoon, X.Q. Yang, Electrochem. Commun. 11 (2009) 913.
[27] D.Y. Wang, H. Li, S.Q. Shi, X.J. Huang, L.Q. Chen, Electrochim. Acta 50 (2005) 2955.
[28] M.R. Yang, W.H. Ke, J. Electrochem. Soc. 155 (2008) A729.
[29] A. Yamada, S.C. Chung, K. Hinokuma, J. Electrochem. Soc. 148 (2001) 224.
[30] H.Y. Gao, L.F. Jiao, W.X. Peng, G. Liu, J.Q. Yang, Q.Q. Zhao, Z. Qi, Y.C. Si, Y.J. Wang, Electrochim. Acta 56 (2011) 9961.
[31] A. Rouier, G.A. Nazri, Ionics 3 (1997) 170.
[32] M.F. Zhou, L.N. Zhang, L.M. Shao, W.N. Wang, K.N. Fan, Q.Z. Qin, J. Phys. Chem. A 105 (2001) 5801.
[33] M.A. Gondal, T.A. Saleh, Q.A. Drmosh, Appl. Surf. Sci. 258 (2012) 6982.
[34] Y. Sundarayya, K.C. Kumara, C.S. Sunandana, Mater. Res. Bull. 42 (2007) 1942.
[35] L. Yang, L. Jiao, Y. Miao, H. Yuan, J. Solid State Electrochem. 13 (2009) 1541.
[36] L.J. Pang, M.S. Zhao, X. Zhao, Y.J. Chai, J. Power Sources 201 (2012) 253.
[37] Y.H. Nien, J.R. Carey, J.S. Chen, J. Power Sources 193 (2009) 822.
[38] G.M. Song, Y. Wu, G. Liu, Q. Xu, J. Alloys Compd. 487 (2009) 214.
[39] X.G. Yin, K.L. Huang, S.Q. Liu, H.Y. Wang, H. Wang, J. Power Sources 195 (2010) 4308.
[40] A.J. Bard, L.R. Faulkner, Electrochem. Methods, Wiley, 2001, p. 231.
[41] H.B. Shu, X.Y. Wang, Q. Wu, B.W. Ju, L. Liu, X.K. Yang, Y.P. Wang, J. Electrochem. Soc. 158 (2011) A1448.
[42] H.B. Shu, X.Y. Wang, Q. Wu, B.W. Ju, Electrochim. Acta 76 (2012) 120.
[43] Y. Cui, X.L. Zhao, R.S. Guo, Mater. Res. Bull. 45 (2010) 844.